JOURNAL OF MAGNETIC RESONANCE **135,** 466–477 (1998)
ARTICLE NO. MN981592

Excitation of Complicated Shapes in Three Dimensions

Igor Serša* and Slobodan Macura†,[1]

*Department of Solid State Physics, Jozef Stefan Institute, 1000 Ljubljana, Slovenia; and †Department of Biochemistry and Molecular Biology, Mayo Graduate School, Mayo Clinic and Mayo Foundation, Rochester, Minnesota 55905

E-mail: macura@mayo.edu

Received February 27, 1998; revised August 21, 1998

We experimentally verified a recently proposed technique for the excitation of a complicated three-dimensional profile (CARVE, *c*ompletely *a*rbitrary *r*egional *v*olume *e*xcitation). CARVE is based on a generalized DANTE RF pulse sequence and a synchronous string of gradient steps. Provided there is no limitation in the number of pulses, CARVE can generate an excitation profile of any shape with any resolution. However, hardware limitations and sample properties restrict the number of RF pulses and gradient steps and, thus, limit attainable resolution of the excitation profile. We theoretically and experimentally showed that spatial resolution can be increased by distributing a long sequence among several CARVE experiments and summing up their signals. This is particularly important for three-dimensional excitation profiles where an *n*-fold increase in resolution requires an n^3-fold increase of the number of events in the sequence. The potential use of three-dimensional CARVE might be in spectroscopic imaging where the excitation profile can be tailored to match the shape of a selected organ or body part. © 1998 Academic Press

Key Words: ***k*-space trajectory; spectroscopic imaging; volume selective excitation.**

INTRODUCTION

The ultimate goal of spectroscopic imaging is to reveal the spatial distribution of chemical species, i.e., to record NMR spectrum as a function of spatial coordinates. For distribution in n dimensions, one must record an $n + 1$-dimensional image where information about chemical shifts is stored in an additional dimension. For three-dimensional (3D) space, spectroscopic imaging requires a 4D image, which is usually time consuming to record. Fast techniques for volume localization provide spectroscopic information only from a single-shaped region, usually a cube or sphere (*1–6*). Thus, fast techniques for spectroscopic imaging that can excite complicated profiles are desirable and have been proposed (*7–9*). We also have proposed a technique for completely arbitrary regional volume excitation (CARVE) in which spatial localization is achieved by use of a generalized DANTE RF pulse sequence (*10*) interleaved with gradient steps (*11–13*).

In this article, we present a theory and implementation of CARVE for on-resonance spins in three dimensions. We focus on experiments with a large number of events typical for 3D and show that in such cases CARVE can be distributed into several experiments with shorter sequences. Each short sequence excites the NMR signal in a way different from the desired profile, but their sum generates the excitation profile with the required resolution. Special care also is taken in the design of the CARVE sequence, with a minimal gradient load.

THEORY

Basic Relations

Under the influence of RF field $B_1(t)$ ($B_1 = B_{1x} + iB_{1y}$) and magnetic field gradient $\mathbf{G}(t)$, spatially distributed magnetization $M_0(\mathbf{r})$ rotates from its initial equilibrium position (along the z axis) and acquires a certain orientation in the rotating frame of reference that is a function of spatial coordinates $\mathbf{r}$ and the time T elapsed. Such magnetization can be conveniently represented over the transverse component $M^+(\mathbf{r}, T)$, and the longitudinal component $M_z(\mathbf{r}, T)$. In the small tip-angle approximation, the complex transverse magnetization, $M^+(\mathbf{r}, T)$ ($M^+ = M_x + iM_y$), can be represented as (*7, 14, 15*)

$$M^+(\mathbf{r}, T) = i\gamma M_0(\mathbf{r}) \int_0^T B_1(t)\exp[+i\mathbf{k}(t)\mathbf{r}]dt, \qquad [1]$$

where $\mathbf{k}(t)$ is proportional to the integral of magnetic field gradient over time

$$\mathbf{k}(t) = -\gamma \int_t^T \mathbf{G}(t')dt'. \qquad [2]$$

[1] To whom correspondence should be addressed. Fax: (507) 284-8433.

1090-7807/98 $25.00

For the discrete case where an RF field is applied as a series of short DANTE pulses and gradient as square steps with step length equal to the RF pulse separation, integrals in Eqs. [1] and [2] can be converted into corresponding sums. If N equidistant pulses are delivered during the interval T, then the spacing between the successive RF pulses is $\Delta t = T/N$ and the total time till lth pulse is

$$t_l = l\Delta t. \qquad [3]$$

Then, the integral in Eq. [2] can be replaced by the sum

$$\mathbf{k}_l = \mathbf{k}(t_l) = -\gamma\Delta t \sum_{j=l}^{N-1} \mathbf{G}_j \qquad [4]$$

with $l = 0, \ldots, N-1$.

If the RF pulses are rectangular and their width τ_p much shorter than the pulse separation $\tau_p \ll \Delta t$, then the amplitude $B_{1,l}$ can be expressed by a complex angle $\Theta_l = \theta_l \exp(i\varphi_l)$ by which magnetization is tipped from the z axis

$$B_{1,l}(t) = \begin{cases} \dfrac{\Theta_l}{\gamma\tau_p}, & l\Delta t < t < l\Delta t + \tau_p \\ 0, & \text{elsewhere.} \end{cases} \qquad \tau_p \ll \Delta t \qquad [5]$$

The relationship between the gradient and RF pulses and their timing in a single event is illustrated in Fig. 1. By substituting the general RF magnetic field $B_1(t)$ in Eq. [1] with the DANTE train of short RF pulses as introduced in Eq. [5] the following excitation profile is obtained:

$$P_N(\mathbf{r}) = \frac{M_N^+(\mathbf{r})}{iM_0(\mathbf{r})} = \sum_{l=0}^{N-1} \Theta_N(\mathbf{k}_l)\exp(+i\mathbf{r}\mathbf{k}_l). \qquad [6]$$

Due to the infinitely short RF pulses the vectors $\mathbf{k}_l$ are discrete, but the real space spanned by vectors $\mathbf{r}$ is continuous. To ease the calculation of Eq. [6] we considered a special case where an ideal profile $P_N(\mathbf{r})$ is defined in a D-dimensional cube with side L, on a matrix of $N = M^D$ equidistant points $\mathbf{r}_n$ that span a rectangular grid. The modulation vectors $\mathbf{k}_l$ are also equidistant within a D-dimensional cube with side $2\pi M/L$. For such vectors $\mathbf{r}_n$ and $\mathbf{k}_l$ Eq. [6] represents the discrete Fourier transform, and the CARVE excitation profile becomes the discrete Fourier transform of the short RF pulses $\Theta_N(\mathbf{k}_l)$ (*12*):

$$P_N(\mathbf{r}_n) = \sum_{l=0}^{N-1} \Theta_N(\mathbf{k}_l)\exp(+i\mathbf{r}_n\mathbf{k}_l). \qquad [7]$$

Conversely, the CARVE sequence that excites the desired profile $P_N(\mathbf{r}_n)$ is the discrete inverse Fourier transform of the discrete profile in real space

$$\Theta_N(\mathbf{k}_l) = \frac{1}{N} \sum_{n=0}^{N-1} P_N(\mathbf{r}_n)\exp(-i\mathbf{r}_n\mathbf{k}_l). \qquad [8]$$

Equation [8] shows that for excitation profile $P_N(\mathbf{r}_n)$ defined with N spatial points one needs N RF pulses Θ_l and N gradient steps (k-space coordinates).

The discrete nature of CARVE also introduces periodicity of the profile. The profile $P_N(\mathbf{r}_n)$ periodically repeats with a period L in all D perpendicular spatial directions.

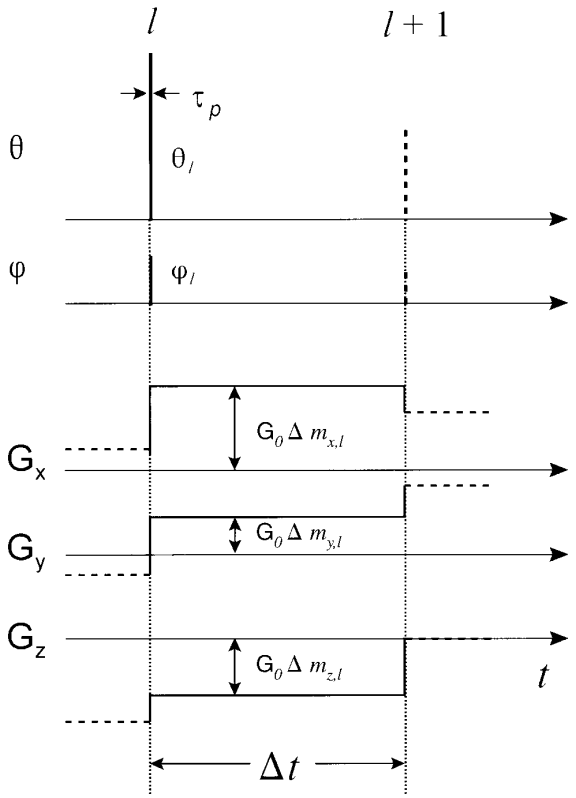

FIG. 1. A single CARVE event consists of short RF pulse and a gradient step. A short RF pulse with flip angle θ, phase φ, and duration τ_p is applied simultaneously with the gradient step (with components G_x, G_y, G_z equal to the integer multiples of the gradient unit magnitude G_0) of duration Δt. Because $\tau_p \ll \Delta t$ effects of the gradient during the RF pulse can be neglected, and the CARVE event may be considered as an RF pulse followed by the gradient pulse, as required by Eqs. [6] and [7].

Distributivity of the Sequence

Because of limited gradient strength, finite gradient slew-rate, and transverse and longitudinal relaxation times, the number of pulses in a single CARVE excitation is limited. This may restrict the use of Eq. [8] to simple shapes. However, linearity of the CARVE sequence enables the excitation of

arbitrary shape by distributing the pulses of a long DANTE sequence into several shorter ones, repeating the experiment with each of these shorter sequences, and accumulating the complex signals obtained from all these experiments. We can rewrite Eq. [7] as

$$P_N(\mathbf{r}_n) = \sum_{s=0}^{N_E-1} \sum_{l=0}^{N_S-1} \Theta_N(\mathbf{k}_{s,l}) \exp(+i\mathbf{r}_n\mathbf{k}_{s,l}) = \sum_{s=0}^{N_E-1} P_{N_S,s}(\mathbf{r}_n), \quad [9]$$

where summation over N coefficients is distributed among N_E experiments each with N_S pulses (elements); partial sums may have an arbitrary number of elements, and the only condition is

$$\sum_{s=0}^{N_E-1} N_S = N. \quad [10]$$

Thus, the excitation profile $P_N(\mathbf{r}_n)$ defined by N elements can be fully reconstructed by summation of all nonoverlapping subprofiles $P_{N_S,s}(\mathbf{r}_n)$, irrespective of their number, size, and distribution in k-space. Distributivity of CARVE stems from its linearity and provides a means to excite a complicated profile with any resolution. It also provides a basis for the excitation profile approximation when the total number of experiments is limited.

Approximation of Excitation Profile

If the total number of available coefficients $\Theta_{N'}$ is smaller than the number of coefficients in the original excitation profile, $N' < N$ ($N = M^D$), then the actual profile $P_{N'}(\mathbf{r}_n)$ represents only an approximation of the original profile $P_N(\mathbf{r}_n)$. A subset of N' coefficients out of N can be chosen in many ways using different criteria. According to Parseval's theorem, the squared norm of ideal excitation profile $\|P_N(\mathbf{r}_n)\|^2$ is equal to the complete sum of squared projections of harmonic functions on the ideal profile. Obviously, the partial sum over selected N' harmonic functions gives a norm $\|P_{N'}(\mathbf{r}_n)\|^2$ lower than the squared norm of the ideal profile. However, maximizing $\|P_{N'}(\mathbf{r}_n)\|^2$ by selecting N' harmonic functions with the highest projection on the ideal excitation profile gives a profile approximation that has the volume closest to the volume of the original. To quantify the fidelity of this approximation, we introduce the resemblance factor η as a ratio of the squared norms of the approximate $P_{N'}$ and the original profile P_N

$$\eta = \frac{\|P_{N'}(\mathbf{r}_n)\|^2}{\|P_N(\mathbf{r}_n)\|^2} = \frac{\sum_{l=0}^{N'-1} |\Theta_l|^2}{\sum_{l=0}^{N-1} |\Theta_l|^2}, \quad [11]$$

where the last ratio is derived by taking the squared norm of Eq. [7]. Apparently the maximal resemblance factor η ($0 \leq \eta \leq 1$) is obtained by taking N', the largest coefficients Θ_l. Indexes of selected coefficients Θ_l also determine a subset of the k-space points that need to be traversed.

Determination of k-Space Walk

The order in which selected k-space points are visited is irrelevant for the quality of the excitation profile because the ordering influences merely the sequence of summation of different terms in Eqs. [7] and [9]. However, the order of k-space points determines the strength of individual gradient steps (Eqs. [4] and [13]). The longer the k-space distance between successive points $\Delta\mathbf{k}_l$, the larger the gradient necessary to traverse that distance within a given interval Δt (Eq. [13]). Because the maximum gradient strength and the slew-rate are the limiting factors, it is desirable to find a walk through k-space points that minimizes gradient load.

Intentionally, we try to avoid using the term "trajectory," because in CARVE, k-space is discrete and points are visited in leaps rather than continuous paths. This offers an advantage compared to continuous k-space because the problem of trajectory crossing is nonexistent. The direct consequence is that the hops between the selected k-space points can be optimized more freely. If all $N = M^D$ points from a given k-space cube are selected, the walk between them can mimic sequential or spiral trajectory. However, if a subset of N' points (out of N points) is selected, other walks may be more effective. Because there is no trajectory, hops between the points in discrete k-space can be optimized to minimize gradient load without any restrictions. Because the subset of selected points $\mathbf{k}_{s,l}$ depends on the number of points N' and on the actual shape of the profile, the walk is custom designed for each case. We have chosen to use a simulated annealing protocol (*16*) to find a walk with the desired properties. The penalty function in the simulated annealing depends on the property that should be optimized. An obvious choice is to minimize the total walk length. Then the penalty function E that needs to be minimized is

$$E \propto \sum_{l=0}^{N'-1} (\Delta\mathbf{k}_l)^2 \quad [12]$$

with

$$\Delta\mathbf{k}_l = \mathbf{k}_l - \mathbf{k}_{l+1} = -\gamma\Delta t\mathbf{G}_l \quad [13]$$

for $l = 0, \ldots, N' - 1$, where $\mathbf{k}_{N'} = 0$. This is equivalent to the minimization of squared gradient load,

$$E \propto \sum_{l=0}^{N'-1} \mathbf{G}_l^2. \quad [14]$$

Such a penalty function is also justified by the proportionality of the accumulated phase during gradient rise/fall period to the square of the gradient amplitude. (The accumulated phase is proportional to the k-space position; thus, an error in accumulated phase propagates as an error in k-space position.) This proportionality is based on the assumption that the gradient increases (decreases) linearly with time during the rise/fall period. Thus, penalty function expressed by Eqs. [12] and [14] generates a walk that minimizes distortions caused by the finite gradient's time constant. Penalty functions that eliminate other possible sources of distortions can be easily designed. Even a coarse minimization of the penalty function is sufficient for most practical purposes. This allows less stringent implementation of a simulated annealing protocol. For example, simulated annealing with fast cooling does not find the deepest minimum but quickly finds others that generate sufficiently efficient walks.

Definition of Excitation Profile $P_N(\mathbf{r}_n)$

An excitation profile is defined as a real space $M \times M \times M$ cube with length L (Fig. 2a). Here we constructed profiles as phantoms, but in real situations the profile is derived from the prerecorded image of the studied object. Then the profile is constructed as one-bit image of the object where all the data outside the region of interest are zeroed. To eliminate oscillations at the edges (Gibbs' phenomenon), the profile can be renormalized to an 8-bit image and smoothed. Then, the excitation profile $P_{M^3}(\mathbf{r}_n)$ is a 3D matrix defined in the (discrete) points $\mathbf{r}_n = (L/M)(u_x, u_y, u_z)$ with coordinates u $(-M/2 \le u \le M/2 - 1)$ relative to the matrix size and centered within the cube

$$P_{M^3}(\mathbf{r}_n) = P_{M^3}\left(\frac{L}{M}u_x, \frac{L}{M}u_y, \frac{L}{M}u_z\right) \equiv P(u_x, u_y, u_z). \quad [15]$$

The profile is defined with M^3 data points. To faithfully reproduce the profile from the prerecorded image, CARVE needs the same number of events, $N = M^3$.

Calculation of $\Theta_N(\mathbf{k}_l)$

According to Eq. [8], $\Theta_N(\mathbf{k}_l)$ is an inverse Fourier transform of the excitation profile (Fig. 2a). Because the excitation profile is defined in a real space within a cube with $M \times M \times M$ elements and size L, the complex RF sequence Θ is defined in the $M \times M \times M$ k-space cube with the length $2\pi M/L$ in discrete points $\mathbf{k}_l = (2\pi/L)(m_x, m_y, m_z)$ and discrete coordinates m $(-M/2 \le m \le M/2 - 1)$

$$\Theta_{M^3}(\mathbf{k}_l) = \Theta_{M^3}\left(\frac{2\pi}{L}m_x, \frac{2\pi}{L}m_y, \frac{2\pi}{L}m_z\right) \equiv \Theta(m_x, m_y, m_z). \quad [16]$$

Then, according to Eq. [8]

$$\Theta(m_x, m_y, m_z) = \frac{1}{M^3}\sum_{u_x,u_y,u_z=-M/2}^{M/2-1}\sum\sum P(u_x, u_y, u_z) \times \exp\left[-i\frac{2\pi}{M}(m_x u_x + m_y u_y + m_z u_z)\right]. \quad [17]$$

Synthesis of Actual Profile $P_{N'}(\mathbf{r}_n)$

The original profile defined by M^3 data points can be approximated with N' points ($N' \ll M^3$), by zeroing all but the N' largest Θ-coefficients, say $\Theta'(m_x, m_y, m_z)$. Then the discrete representation of the excitation profile (actual experimental profile) is obtained by

$$P'(u_x, u_y, u_z) = \sum_{m_x,m_y,m_z=-M/2}^{M/2-1}\sum\sum \Theta'(m_x, m_y, m_z) \times \exp\left[+i\frac{2\pi}{M}(m_x u_x + m_y u_y + m_z u_z)\right]. \quad [18]$$

Thus, the actual experimental profile is the discrete Fourier transform of $\Theta'(m_x, m_y, m_z)$ a matrix with size M^3 (the same as the original matrix $\Theta(m_x, m_y, m_z)$) and which contains the N' largest Θ-coefficients preserved and zeros everywhere else (Fig. 2a). An ideal profile without internal structure has the largest Θ-coefficients clustered around the k-space origin. After selecting the N' largest Θ-coefficients, most of the zeroed coefficients are far from the origin which makes the approximated profile P' look like the low-pass filtered ideal profile.

Optimization of k-Space Walk

The real space and the k-space are the Fourier transform conjugate pair spaces, and their unit vectors are related as $\mathbf{r}^0\mathbf{k}^0 = 2\pi/M$, where $\|\mathbf{r}^0\| = L/M$ and $\|\mathbf{k}^0\| = 2\pi/L$. An arbitrary vector in k-space $\mathbf{k}_l$, expressed over the integer coordinates m $(-M/2 \le m \le M/2 - 1)$, is

$$\mathbf{k}_l = m_{x,l}\mathbf{k}_x^0 + m_{y,l}\mathbf{k}_y^0 + m_{z,l}\mathbf{k}_z^0 = \frac{2\pi}{L}\mathbf{m}_l. \quad [19]$$

Then

$$\left.\begin{aligned}\Delta\mathbf{k}_l &= \frac{2\pi}{L}\Delta\mathbf{m}_l \\ \Delta\mathbf{m}_l &= \mathbf{m}_l - \mathbf{m}_{l+1} \\ \Delta\mathbf{m}_{N-1} &= \mathbf{m}_{N-1}\end{aligned}\right\} l = 0, \ldots, N-2, \quad [20]$$

where $\Delta\mathbf{m}$'s are new integers that describe the difference

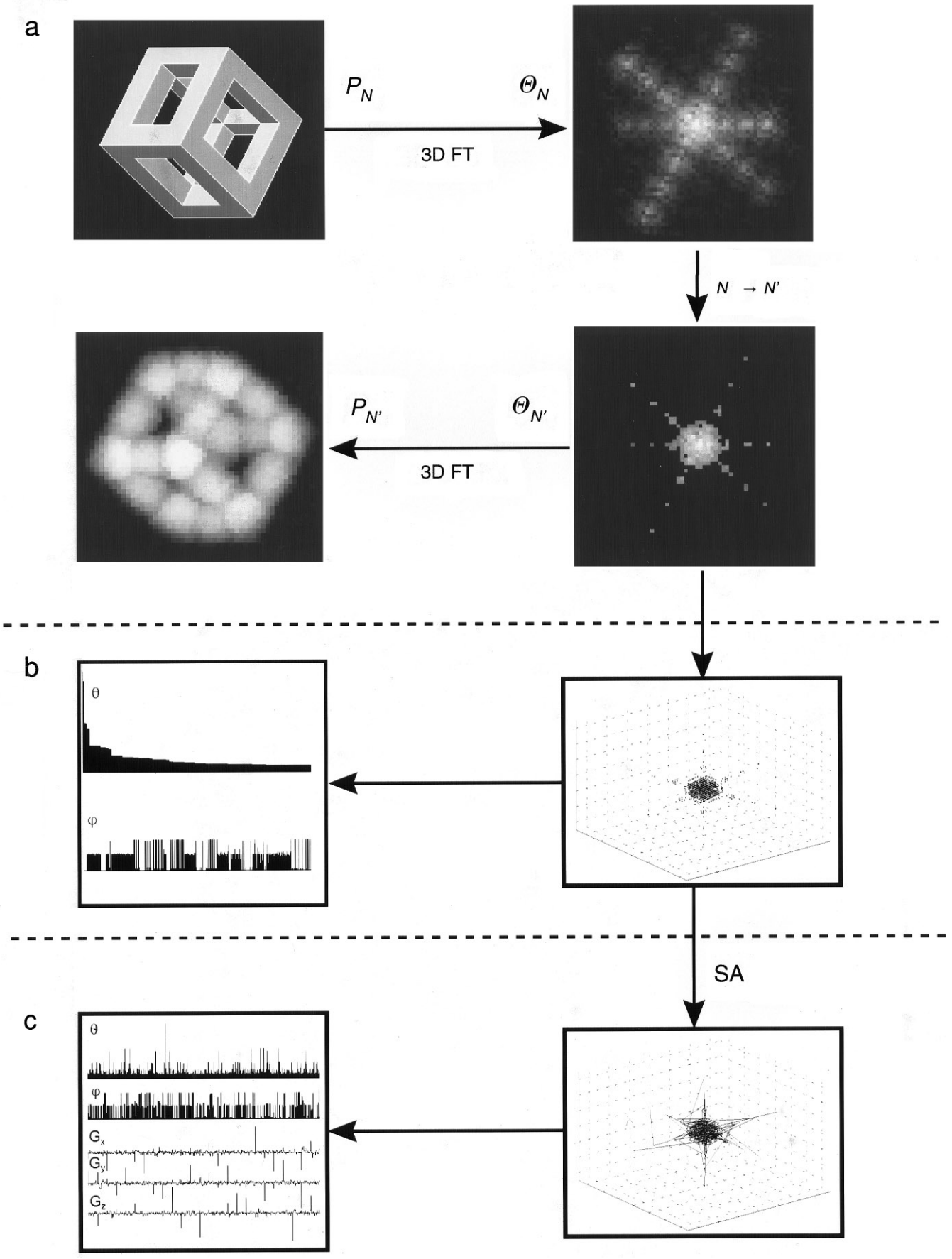
a
P_N
Θ_N
3D FT
$N \rightarrow N'$
$P_{N'}$
$\Theta_{N'}$
3D FT
b
θ
φ
SA
c
θ
φ
G_x
G_y
G_z

between the coordinates of successive points in the k-space walk. Substitution from Eq. [20] into Eq. [13] indicates the gradient step magnitude $\mathbf{G}_l$ necessary to reach any k-space point

$$\mathbf{G}_l = -\frac{2\pi}{\gamma \Delta t L}\,\Delta \mathbf{m}_l = -G_0 \Delta \mathbf{m}_l, \qquad [21]$$

where the smallest gradient step depends on the size of excitation window L and the gradient step duration Δt

$$G_0 = \frac{2\pi}{\gamma \Delta t L}. \qquad [22]$$

Then the penalty function that minimizes gradient load according to Eqs. [12] and [14] is

$$E \propto \sum_{l=0}^{N'-1} [(\Delta m_{x,l})^2 + (\Delta m_{y,l})^2 + (\Delta m_{y,l})^2]. \qquad [23]$$

Similarly, if the pulse sequence is distributed among N_E experiments with N_S pulses, the penalty function becomes

$$E \propto \sum_{s=0}^{N_E-1} \sum_{l=0}^{N_S-1} \mathbf{G}_{s,l}^2$$

$$\propto \sum_{s=0}^{N_E-1} \sum_{l=0}^{N_S-1} [(\Delta m_{x,s,l})^2 + (\Delta m_{y,s,l})^2 + (\Delta m_{z,s,l})^2]. \qquad [24]$$

The main difference between Eqs. [23] and [24] is that in the latter constraints between the individual segments (s and $s + 1$) are removed. Because they belong to different experiments, successive gradient steps are unrelated.

Once the set of N' coefficients Θ_l is selected, actual tip angles θ_l (measured from the z axis), and phases φ_l (measured from the x' axis of the receiver) are calculated by use of Eq. [17]:

$$\Theta_l = \theta_l \exp(i\varphi_l). \qquad [25]$$

If the Θ_l coefficients are selected using a squared norm (Eq. [11]), then the events are already sorted by the tilt angle (Fig. 2b).

A sequence whose events are sorted according to the size of the tip angle in theory is as good as any other, but in practice, it may produce a distorted profile because of too large a gradient load (*13*). To minimize the load on the gradient system, individual events are reshuffled until the chosen penalty function is minimized (Fig. 2c). This generates a sequence of events that produces an excitation profile with minimal distortions.

RESULTS

We present computer simulations and experimental verification of the distributive character of the CARVE sequence and its feasibility in three dimensions.

High Definition 2D CARVE

To demonstrate the distributive character of the CARVE sequence we generated a complicated 2D excitation profile $c_a{}^R v^e$ that requires a large number of events to be reproduced faithfully. The original profile is depicted in Fig. 3b and its approximation with 1000 coefficients in Figs. 3c and 3e. A sequence with 1000 events would last 0.5 s, and in practice not much magnetization would be detected afterward. Instead of running a 1000-pulse experiment it is better to distribute the sequence among several experiments with a smaller number of pulses. To push it to the end we distributed the sequence among 1000 independent one-pulse experiments. The resulting profile is obtained as a sum of 1000 individual subprofiles (Figs. 3d, 3f). A comparison of Figs. 3c, 3e and 3d, 3f clearly shows high fidelity of reproduction of a rather complicated shape by a long CARVE sequence that is distributed among several experiments.

Distributivity of 3D CARVE Excitation

The only difference between 2D and 3D CARVE experiments is that in 3D the number of necessary coefficients is always too large for the sequence to be executed in a single experiment. Thus, a distribution of the sequence among several experiments is inevitable. To demonstrate this, we performed a series of simulations using a cubic box frame as an ideal profile. Besides the ideal profile ($N = \infty$), Fig. 4a shows the same profile approximated with a different number of Fourier coefficients N'. For a given profile, a fair approximation is obtained only with a few hundred coefficients. To visualize how additional coefficients improve the actual profile, Fig. 4a shows the profile defined with 500 coefficients separated into five profiles of 100 coefficients. Profiles are sorted according to the magnitude of the coefficients. Thus, the first profile in Fig. 4b is the same as that in Fig. 4a with $N' = 100$. The other

FIG. 2. The CARVE sequence pulse design. (a) The sampled original profile P_N is Fourier transformed (FT), and the set of N' coefficients is selected. Fourier transform from k-space into real space generates an approximative profile P_N, which represents the best one could obtain with a given number of coefficients. (b) Selected k-space coefficients yield radio frequency tip angles and phases. (c) The k-space coordinates of selected coefficients yield corresponding gradient steps. To minimize gradient load, k-space walk is optimized by simulated annealing (SA).

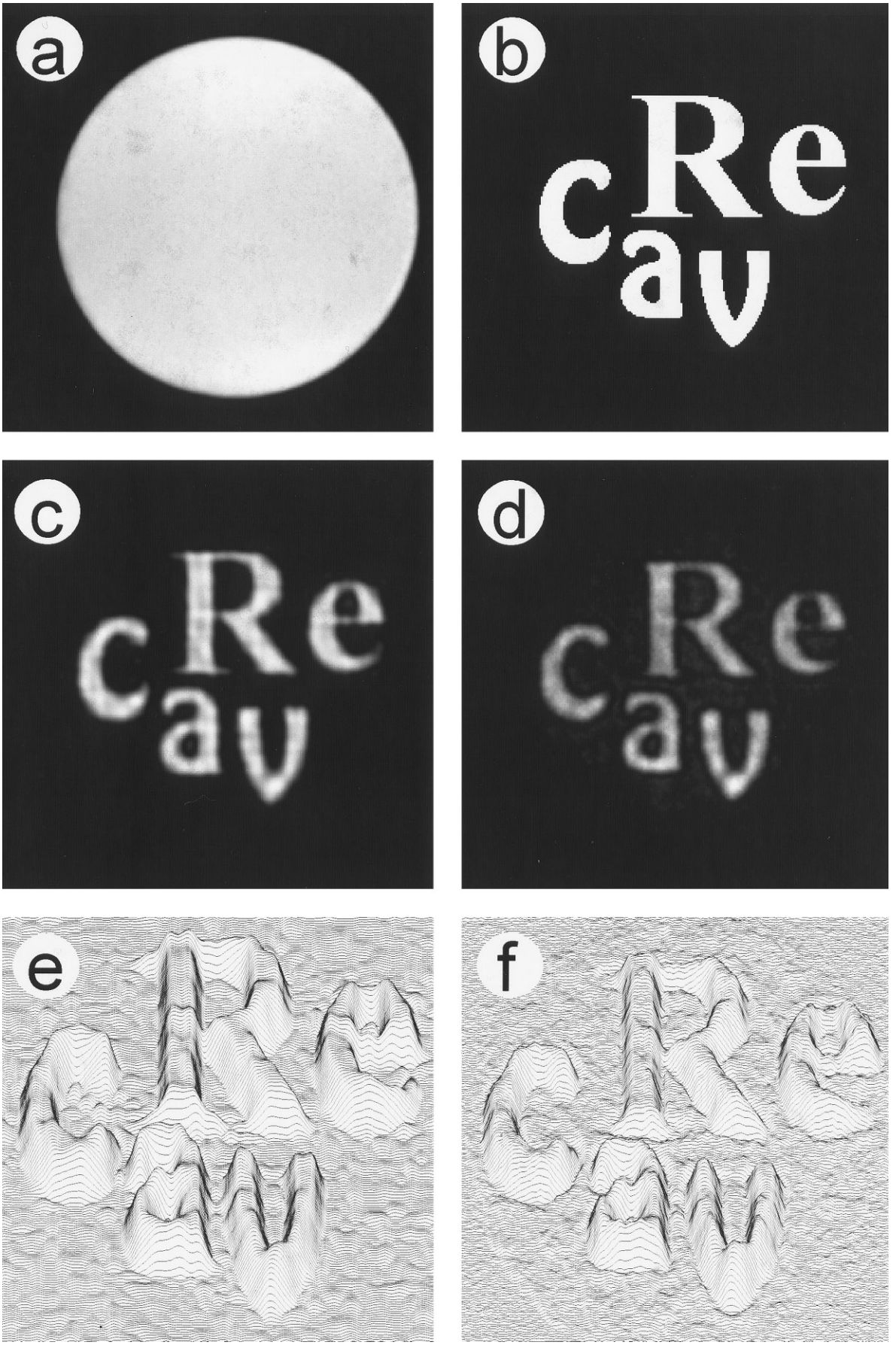
a
b
Re
c
a v
c
Re
c
a v
d
Re
c
a v
e
f

profiles, as sets of the coefficients with smaller magnitude, are just small corrections of the one with the largest coefficients. Their sum gives the profile from Fig. 4a with $N' = 500$. Finally, Fig. 4c shows the same 500-coefficient profile distributed again among five 100-coefficient profiles. This time, however, coefficients sets were grouped by the *k*-space walk optimization (by simulated annealing) that distributed the largest coefficients evenly among different subprofiles. Neither subprofile resembles the 500 approximation, but their sum matches it exactly as does the sum of the subprofiles in Fig. 4b.

Thus, the distributive character of the CARVE excitation enables improvement of the profile approximation by co-addition of the result of several independent experiments. When many scans need to be collected, for example because of low sensitivity, improvement in the excitation profile approximation can be achieved without prolonging the total experimental time.

Experimental Verification of Distributed 3D CARVE Excitation

For a 500-coefficient approximation of the original cubic frame profile (Fig. 4a), RF pulse tilt angles and phases are calculated from the largest coefficients as depicted in Fig. 2. The *k*-space coordinates of the largest 500 coefficients are shown in Fig. 5a. The total time of 250 ms to visit all *k*-space points is prohibitively long; thus, the sequence is split into 25 experiments with 20 pulses each. With use of the penalty function expressed by Eq. [24], 25 *k*-space walks that minimize the gradient load are constructed (Fig. 5b); Fig. 5c shows 6 walks on an expanded scale. These determine the order of RF pulses and gradient steps, which are shown in Fig. 5d.

Figure 6 shows the ideal (6a), simulated (6b), and experimental (6c) cubic frame profiles. A good match is evident between the simulated and experimental profiles, which demonstrates the feasibility of complicated shape excitation by distributing long CARVE sequences among several independent experiments.

DISCUSSION

The CARVE sequence is based on the Fourier transform relationship between the real space excitation profile and its excitation pulse sequence (Eqs. [7] and [8]); therefore, CARVE is also linear. Here we focus on experimental verification of the distributive character of CARVE; we analyzed other properties elsewhere (*13*). The distributive character of CARVE follows from Eq. [7], which states that the profile in real space is obtained by summing the effects of short RF pulses (generalized DANTE sequence) fired at particular *k*-space points. The only restriction is the pairwise correspondence between the complex RF angles Θ and *k*-space coordinates; the sequence of RF pulses and corresponding *k*-space points can be executed in any order and in any combination. This means that the experimental profile obtained with any subset of (Θ, $\mathbf{k}$) pairs can be further improved by adding subprofiles from unused (Θ, $\mathbf{k}$) pairs. Again, the order in which pairs are added and their number can vary without restriction.

Extreme cases are the profile excitation in a single experiment with *N* events (Θ, $\mathbf{k}$) or in a series of *N* experiments each with a single (Θ, $\mathbf{k}$) event. These cases are equivalent theoretically, but practically thus are quite different. A single experiment has an advantage of exciting the profile quickly but a disadvantage is sensitivity to the hardware and the sample limitations. On the other hand, in a series of experiments with the single (Θ, $\mathbf{k}$) event, neither the properties of the sample nor the properties of the hardware are challenged, but the experiment is prohibitively time consuming. (For simplicity, we consider only on-resonance magnetization and neglect the effects of the excitation bandwidth.) Apparently, the suitable compromise could always be found; the number of experiments and the number and the distribution of the (Θ, $\mathbf{k}$) events can be tailored to suit a particular application. For example, recording of the ^{13}C spectrum in natural abundance usually requires several thousand scans. Then the spatial selectivity can be incorporated without compromising the basic experiment, by replacing a single excitation pulse with a single (Θ, $\mathbf{k}$) event and by launching a new event in every scan. On the other hand, if one wants to record a frequency-selective proton signal that might be acquired in a few scans, then an excitation pulse is replaced by a sequence of (Θ, $\mathbf{k}$) events which can be the same or different for each scan. The number of events depends on the required selectivity and on the hardware properties.

CONCLUSION

We have demonstrated experimentally the feasibility of exciting a complicated 3D profile by a CARVE sequence with arbitrarily high resolution. The method uses the distributive character of the CARVE sequence. The desired excitation profile is obtained as a superposition of several subprofiles obtained in independent experiments. The number and properties of the subprofiles can be customized for

FIG. 3. Excitation of a complicated profile in two-dimensions with 1000 one-event CARVE experiments. (a) Experimental cross section of a 5-mm NMR tube filled with water and recorded with uniform spatial excitation. (b) Synthetic profile P_N, defined as a one-bit image in a 256 × 256 matrix; $N = 65{,}536$. (c) Approximate profile P_N, obtained by 2D inverse Fourier transform of the 1000 largest coefficients from the *k*-space image of the original profile. (d) Experimental excitation of profile (c). (e) Stacked plot of the 1000 coefficients profile from (c). Background noise and character distortions are due to limited number of coefficients used. (f) Stacked plot of experimental profile (d). It is evident that the experimental profile faithfully reproduces most of the distortions due to the limited number of coefficients.

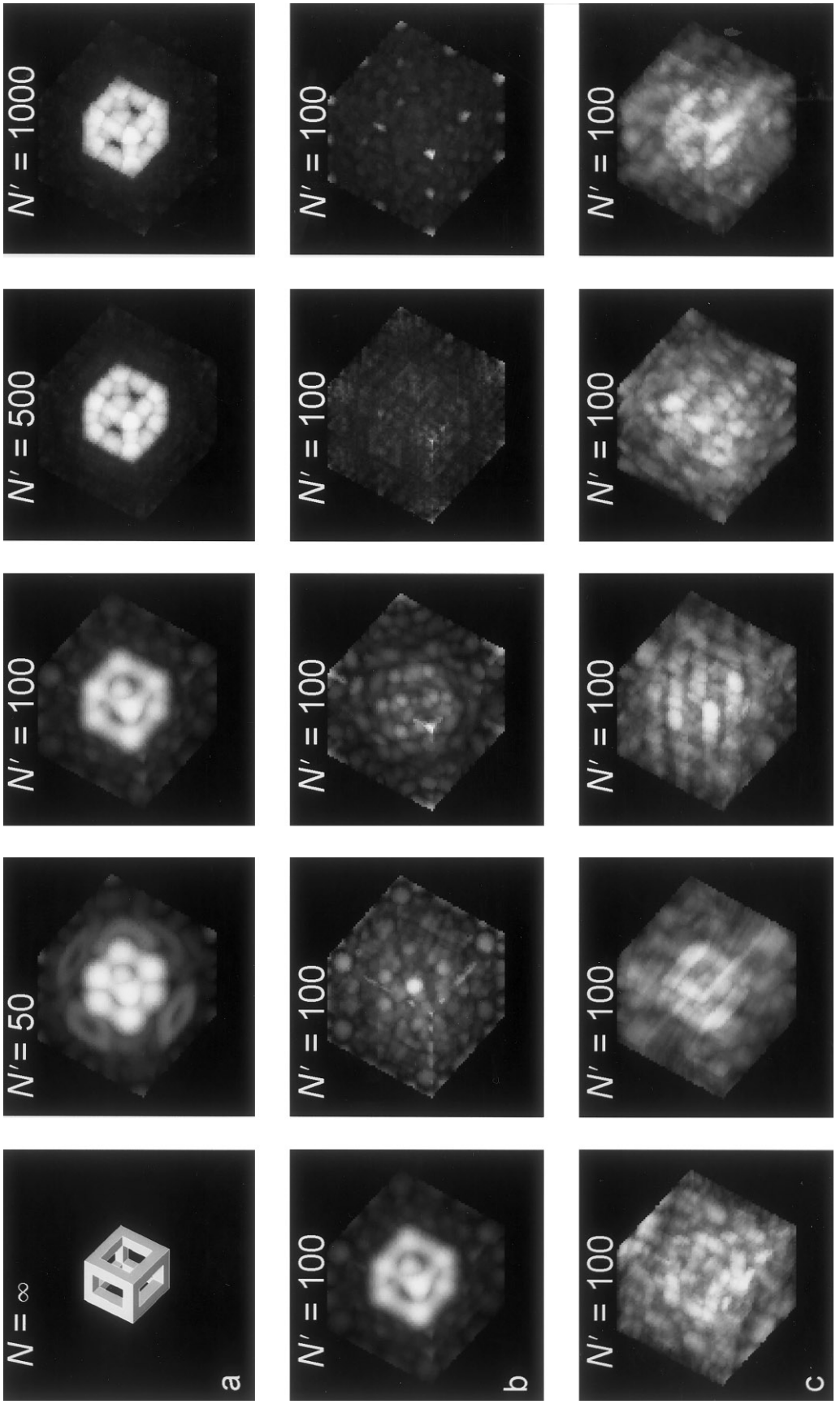

FIG. 4. Simulated excitation profiles of 3D box frame. (a) Ideal box frame ($N = \infty$) and its representation with a different number of coefficients, N'. (b) The box frame ($N' = 500$) distributed among five 100-coefficient frames where coefficients are sorted according to their size. The first frame is the same as $N' = 100$ from the top row; their sum yields the frame with $N' = 500$ from the top row. (c) The same frame ($N' = 500$) distributed among five 100-coefficient frames where coefficients are distributed in five groups by simulated annealing to minimize gradient load. The original frame is hardly recognized in the individual images, but the sum of images generates the frame with $N' = 500$ from the top row. For convenience, all images are shown in an absolute value mode, whereas their addition is performed in a phase-sensitive mode.

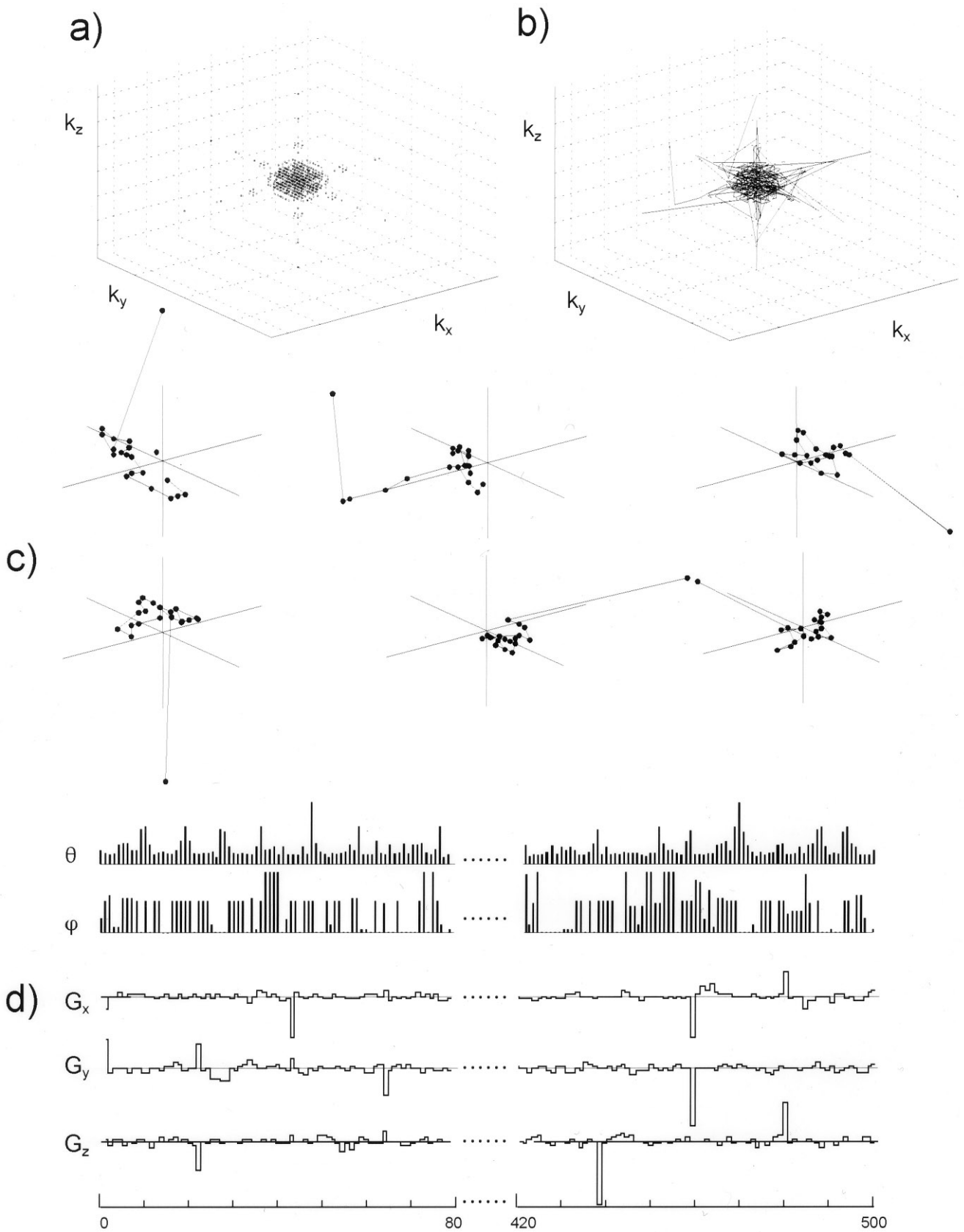

FIG. 5. The pulse sequence design for the box frame excitation profile of 500 events. (a) 500 *k*-space points with the largest Θ-coefficients. (b) *k*-space trajectories. (c) Six (of 25) *k*-space trajectories distributed into groups with 20 points each. (d) Radiofrequency pulse tilt angles θ, phases φ, and gradients. Actual events are distributed into 25 experiments with 20 events each.

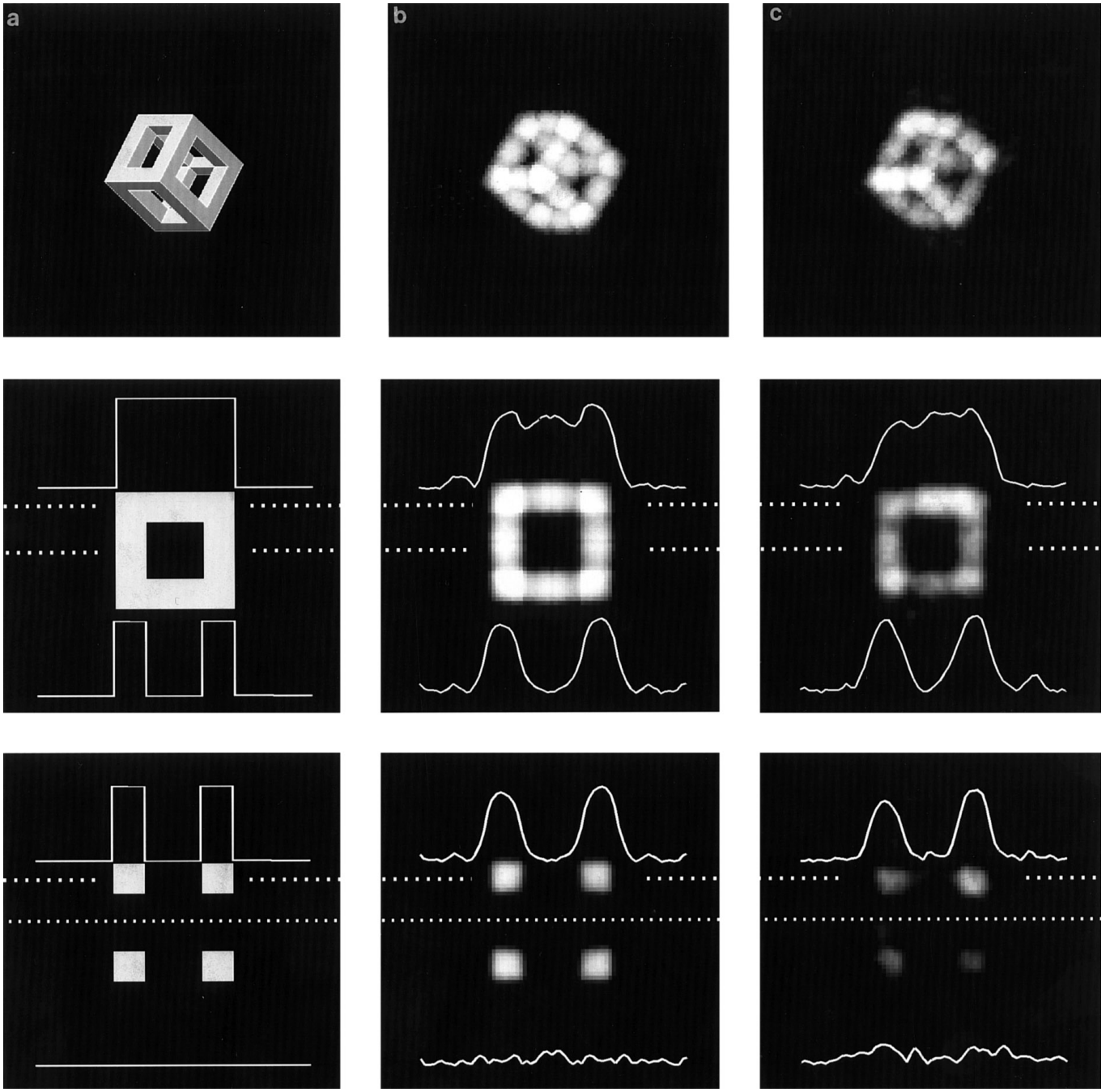

FIG. 6. (a) Ideal (P_∞), simulated (P_{500}), and experimental (P_{500}) box frame excitation profiles. Skewed projection and two cross-sections are shown for each. Time domain data from 25 different experiments are coadded in place during data acquisition. Dashed lines indicate positions at which displayed cross-sections are taken. Cross-sections in (b) and (c) resemble the low-pass filtered cross-sections in (a) due to the low-pass filtering imposed by the criterion for approximation of the profile (Eq. [11]).

particular applications. An approximation by which the desired profile is excited can be improved by successive addition of higher order corrections recorded in subsequent experiments. The distributive character of the CARVE sequence increases its versatility for diverse experiments with volume-selective excitation of arbitrarily complicated shapes.

EXPERIMENTAL

Experiments were performed on a Bruker AMX 300 wide-bore high-resolution spectrometer equipped with microimaging accessories and in a 5-mm tube filled with water. Experimental profiles were visualized by standard 2D or 3D spin-

echo imaging sequences in which the first excitation pulse has been replaced by the CARVE sequence. Time duration per single event (small tip angle RF pulse plus gradient step) Δt was kept to 500 μs to eliminate the effects of finite gradient slew rates. This also kept gradient load within 30% of the maximal gradient, 150 vs 500 mT/m.

ACKNOWLEDGMENT

We thank Dr. Zsolt Zolnai and one of the referees for constructive criticism and many useful suggestions.

REFERENCES

1. S. Mueller, W. P. Aue, and J. Seelig, Practical aspects of volume-selective excitation (vse). Compensation sequences, *J. Magn. Reson.* **65,** 332–338 (1985).
2. W. P. Aue, S. Muller, T. Cross, and J. Seelig, Volume-selective excitation. A novel approach to topical NMR, *J. Magn. Reson.* **56,** 350–354 (1984).
3. J. Frahm and W. Haenicke, Comparative study of pulse sequences for selective excitation in NMR imaging, *J. Magn. Reson.* **60,** 320–332 (1984).
4. P. Bottomley, Selective Volume Method for Performing Localized NMR Spectroscopy. U.S. Patent 4,480,228 (1984).
5. D. Doddrell, J. Bulsing, G. Galloway, W. Brooks, J. Field, M. Irving, and H. Baddeley, Discrete isolation from gradient-governed elimination of resonances. DIGGER, a new technique for *in vivo* volume-selected NMR spectroscopy, *J. Magn. Reson.* **70,** 319–326 (1986).
6. D. M. Doddrell, W. M. Brooks, J. M. Bulsing, J. Field, M. G. Irving, and H. Baddeley, Spatial and chemical-shift-encoded excitation. SPACE, a new technique for volume-selected NMR spectroscopy, *J. Magn. Reson.* **68,** 367–372 (1986).
7. C. H. Meyer, J. M. Pauly, A. Macovski, and D. G. Nishimura, Simultaneous spatial and spectral selective excitation, *Magn. Reson. Med.* **15,** 287–304 (1990).
8. G. Morrell and A. Macovski, Three-dimensional spectral-spatial excitation, *Magn. Reson. Med.* **37,** 378–386 (1997).
9. D. Spielman, J. Pauly, A. Macovski, and D. Enzmann, Spectroscopic imaging with multidimensional pulses for excitation: SIMPLE, *Magn. Reson. Med.* **19,** 67–84 (1991).
10. G. Morris and R. Freeman, Selective excitation in Fourier transform nuclear magnetic resonance, *J. Magn. Reson.* **29,** 433–462 (1978).
11. I. Sersa and S. Macura, Completely arbitrary regional volume excitation (CARVE) by a gradient optimized walk in discrete *k*-space, *in* "Proceedings of the International Society for Magnetic Resonance in Medicine, Fourth Scientific Meeting and Exhibition," Vol. 2, pp. 1224–1224, New York, 1996.
12. I. Sersa and S. Macura, Excitation of arbitrary shapes in nuclear magnetic resonance by a random walk in discrete *k*-space, *J. Magn. Reson. B* **111,** 186–188 (1996).
13. I. Sersa and S. Macura, Excitation of arbitrary shapes by gradient optimized random walk in discrete *k*-space, *Magn. Reson. Med.* **37,** 920–931 (1997).
14. J. Pauly, D. Nishimura, and A. Macovski, A *k*-space analysis of small-tip-angle excitation, *J. Magn. Reson.* **81,** 43–56 (1989).
15. J. Pauly, D. Nishimura, and A. Macovski, A linear class of large-tip-angle selective excitation pulses, *J. Magn. Reson.* **82,** 571–587 (1989).
16. N. Metropolis, A. W. Rosenbluth, M. N. Rosenbluth, A. H. Teller, and E. Teller, Equation of state calculations by fast computing machines, *J. Chem. Phys.* **21,** 1087–1992 (1953).